Int. J. Electrochem. Sci., 14 **(2019)** 5726 – 5737, doi: 10.20964/2019.06.04

International Journal of
ELECTROCHEMICAL
SCIENCE
www.electrochemsci.org

Effect of Bilayer Period on Corrosion Resistance Behavior of CrN/Cr Nanomultilayers Grown On 304 ss

Y. Chipatecua[1], *G. Vazquez*[2], *J.J Olaya*[3]

[1] CINVESTAV-Unidad Queretaro, Qro, 76230, Mexico
[2] Instituto Mexicano del Petróleo, Eje Central Lázaro Cárdenas Norte 152, México City 07730, Mexico
[3] Department of Mechanical and Mechatronic Engineering, Faculty of Engineering, Universidad Nacional de Colombia, 14490, Bogotá, Colombia
*E-mail: ychipatecua@cinvestav.mx

Received: 27 November 2018 / *Accepted:* 19 February 2019 / *Published:* 10 May 2019

CrN/Cr nano-multilayer films grown by using unbalanced magnetron sputtering (UBMS) on 304 stainless-steel (304 ss), varying the bilayer period (Λ) with 20, 100 and 200 nm, and a total thickness of about 1 µm. In this study, the influence of the bilayer period on the electrochemical properties of these films have been investigated. The corrosion resistance of these films was studied by means of electrochemical impedance spectroscopy (EIS) in a 3.0% NaCl solution at room temperature, varying the immersion time from 1 to 168 of constant immersion. The performance of the CrN/Cr nano-multilayer was enhanced with the period increase, which can be attributed to the formation of a dense passive layer. This multilayer architecture hinds columnar film growth resulting in better corrosion resistance.

Keywords: Corrosion, CrN/Cr nanomultilayers, 304 stainless-steel, electrochemical impedance spectroscopy.

1. INTRODUCTION

The thin films deposited by surface modification are a relevant industrial process, used to protect the substrate of corrosion phenomena, wear and fatigue related to the superficial damage. Currently, due to the low cost, highly efficient and the possibility of large-scale production, the electrochemical processes are widely used to obtain hard chromium coatings. However, these technologies generate high hydric and atmospheric contamination, and health cancerogenic problems due to hexavalent chromium vapors (Cr^{+6}) emitted from the CrO_3 solutions employed by this process [1–5].

Nowadays, in surface engineering, the Physical Vapor Deposition (PVD) processes are widely employed to obtain hard coatings with better mechanical, optical and electrical properties. The PVD processes have high flexibility for designing thin films, with a chemical composition and microstructure required as a function of the process parameters [6–9]; thus, it is possible to have a higher process control to grow films with properties according to a specific application. Among the PVD techniques, based on target erosion and assisted by plasma, is found the unbalanced magnetron sputtering (UBMS) results in better quality of the films; because this configuration, with the magnetic field unbalanced, allows the increase of the ion bombardment on the target surface, thus; the density, hard and resistance of the film [8,10,11].

The transition metal nitrides (TMN) deposited by PVD techniques increments significantly the lifetime and quality of the substrates, due to the increase of mechanical properties and corrosion resistance [6,8,12]; however, this high corrosion resistance is reduced due to the corrosive environment attack by a diffusion process through films defects, such as micro-cracks, pores, grain limits, etc. These defects generate direct pathways, where the electrolyte (the NaCl corrosive solution) can diffuse toward the film/substrate interface, altering the electrochemical behavior of the films and reducing its corrosion resistance [11,13,14].

In the last three decades, many studies have been focused on developing multilayer architectures, with nanometric individual layers for increasing the mechanical properties, corrosion and wear resistance, with better properties than one thicker monolayer film. This multilayer architect generates inter-phases which act as barriers for dislocations, reducing the micro-cracks expansion, and thus, increasing the adherence and hardness, while the stress and strain in the films are reduced [15–18].

Past research studies based on CrN/Cr multilayers [15,16,19,20] have been focused on wear resistance, the friction coefficient (COF), Young's modulus, hardness, adherence, and compressive residual stress, correlating these properties with the changes on the bilayer period. Currently, there are no reports in the literature based on CrN/Cr nano-multilayers deposited by UBMS, relating the bilayer period and thickness with the corrosion resistance behavior. The aim of the present study is to evaluate the CrN/Cr nano-multilayers resistance corrosion behavior, as a function of the bilayer period.

2. EXPERIMENTAL

2.1 Thin-films deposition

CrN/Cr nano-multilayers were deposited by using unbalanced magnetron sputtering. The films were deposited on 304 stainless-steel, 2.0x2.0 cm^2, which were wet-polished to a mirror finish. Also, silicon substrates were employed to study the multilayers cross-section. Finally, the substrates were ultrasonically cleaned in acetone and ethanol, for two minutes each one.

A high purity target of Cr (99.99 %) was used, the target-substrate distance was 5.0 cm, and the system base pressure was 1x10^{-4} Pa. Cr films were deposited in a pure Ar atmosphere and CrN films were deposited in Ar-N$_2$ reactive mixtures having 3:1 flow rate, and 7x10^{-1} Pa deposit pressure. Discharge power was ~150 W, and the plasma current was 400 mA for both Cr and CrN as described in [5]. The CrN/Cr nano-multilayers, 1-μm-thick (f) as determined by profilometry measurements, were grown with bilayer period (ʌ) ranging from 20 to 200 nm. This film grow conditions are summarized in Table 1.

Table 1. Period of CrN/Cr nano-multilayers grown on 304 stainless-steel and silicon substrates.

Name	System	Period ʌ (nm)	N° periods (N)
M20	CrN/Cr/304 ss_1	20	50
M100	CrN/Cr/304 ss_2	100	10
M200	CrN/Cr/304 ss_3	200	5

2.2 Thin-films structural characterization

The film structure and preferred growth orientation of CrN/Cr nano-multilayers were determined by X-ray diffraction (XRD), using Cu Kα radiation in Bragg-Brentano mode in a X-PertPro Panalytical equipment. Cross-sectional morphology of films deposited on Si (100) substrates, and superficial morphology deposited on 304 ss substrates (before and after corrosion measurements), were studied using a FEI QUANTA 200 scanning electron microscope. The topography before electrochemical tests, was examined using atomic force microscopy in contact mode, with an Autoprobe CP Park as described in [5]. After EIS measurements, CrN/Cr films topography was analyzed using a laser confocal microscope (LCM) with a solid-state laser of 455 and 550 nm.

2.3 Electrochemical measurements

The corrosion resistance of the CrN/Cr nano-multilayers, grown on polished 304 stainless-steel substrates, was studied in a conventional electrochemical cell using a saturated calomel electrode (SCE) in room-temperature 3.0% NaCl solution with a Gamry potentiostat. EIS measurements were performed at open-circuit potential (OCP). A sinusoidal potential of 10 mV amplitude was applied at frequencies from 10^{-2} to 10^{3} Hz. The results were acquired as a function of NaCl aqueous solution exposure times: 1, 24, 48, 72 and 168 h. Fits to EIS data were made with the Gamry Echem Analysis software [21] using the non-linear least squares method.

3. RESULTS AND DISCUSSION

3.1 Surface characterization

According to the grazing incident angle XRD diffractograms in Fig. 1, the CrN/Cr nano-multilayers mainly consist of the face-centred cubic (fcc) CrN solid phase, with multiple orientations of (111) and (200) peaks with 2θ positions at 37.53 and 43.77°, respectively. The body-centred cubic (bcc) structure α-Cr phase of (110) peak is at 44.39° 2θ position [5], which is the interlayer from each multilayer. The (111) peak for austenite (ɣ-Fe) at 43.58° 2θ position could overlap with Cr (110) and CrN (200) peaks as the film thickness increases while the period is reduced, related to an increase in the number of interfaces. Cr (110) peak intensity increases as interfaces are reduced because of a decrease in the grain size, suggesting higher crystallinity in these films. The deconvolution (not shown) exhibits that the CrN (200) and Cr (110) peaks positions shifted at lower 2θ positions as bilayer period increases, associated with compressive stress usual for multilayer grown by sputtering as have been reported by other studies [14,22–24].

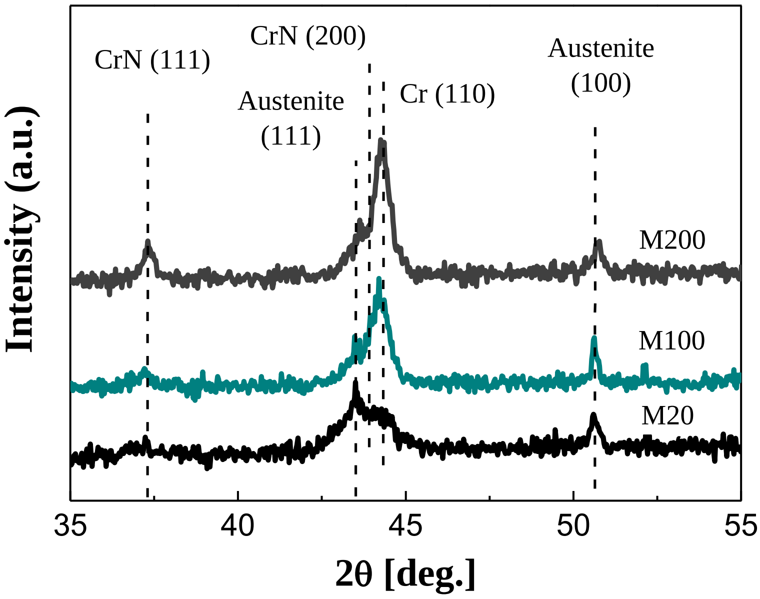

Figure 1. XRD patterns from CrN/Cr nano-multilayers deposited on 304 ss substrates.

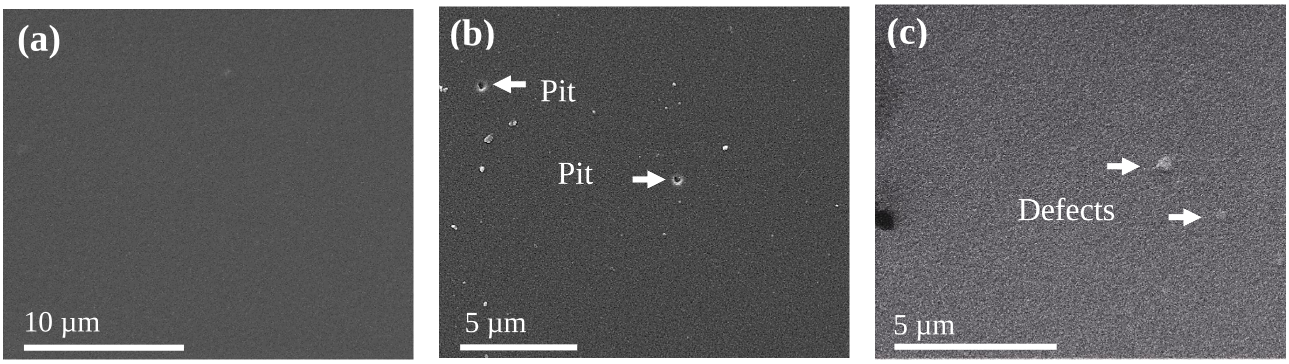

Figure 2. Plain-view SEM image of surface morphology of CrN/Cr nano-multilayers deposited on 304 ss substrates.

PVD coatings usually displays either conical or globular features, pin-holes, pores and other open voids, generated during the deposition process [25]. Their size and density depend upon the deposition conditions [26], however, the permeable defects are more detrimental to the corrosion performance, causing direct pathways to allow the corrosive electrolyte diffusion to reach the film/substrate interface [26]. Fig. 2 shows plan-view SEM images for 1µm-nm-thick CrN/Cr nano-multilayers coated 304 ss substrates with period of 20, 100 and 200 nm (a, b and c, respectively). The films show no evidence of local delamination or micro-crack formation. Fig. 2b shows some pits, these are common defects in PVD coatings [26], while Fig. 2c exhibits some micro-droplets defects [13,25].

Fig. 3 shows the cross-section SEM images of the CrN/Cr nano-multilayers deposited on Si (100) substrates with bilayer period of 100 (Fig. 3a) and 200 nm (Fig. 3b). Light layers correspond to Cr and dark ones to CrN. For all samples studied Cr was the first layer deposited on the substrate, in order to create a transition zone for increasing the adherence and reduce residual stresses due to crystal structure mismatch between the 304 ss substrate and the film [27], and the last layer was CrN. All samples showed a dense multilayer structure without detachment between layers, and between film/substrate, with columnar growth interrupted by interfaces formation layer by layer, corresponding at the T zone of Thornton's structure zone model (SZM) [28].

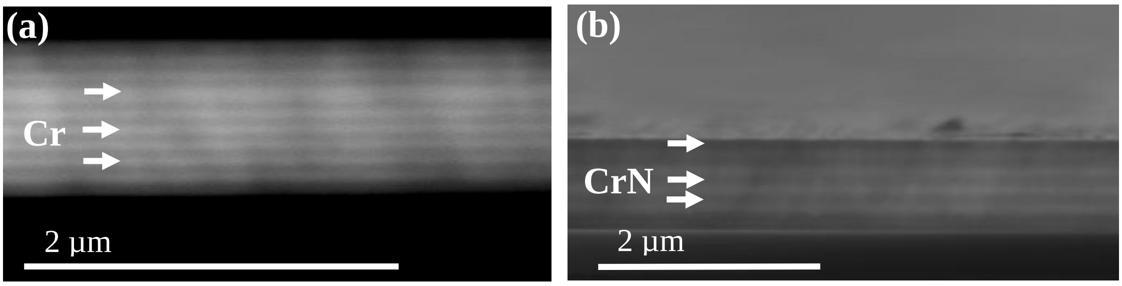

Figure 3. Cross-section SEM images of CrN/Cr nano-multilayers deposited on Si substrates, with period of: (a) Λ = 100 nm and (b) Λ = 200 nm. Light layers correspond to Cr and dark ones to CrN.

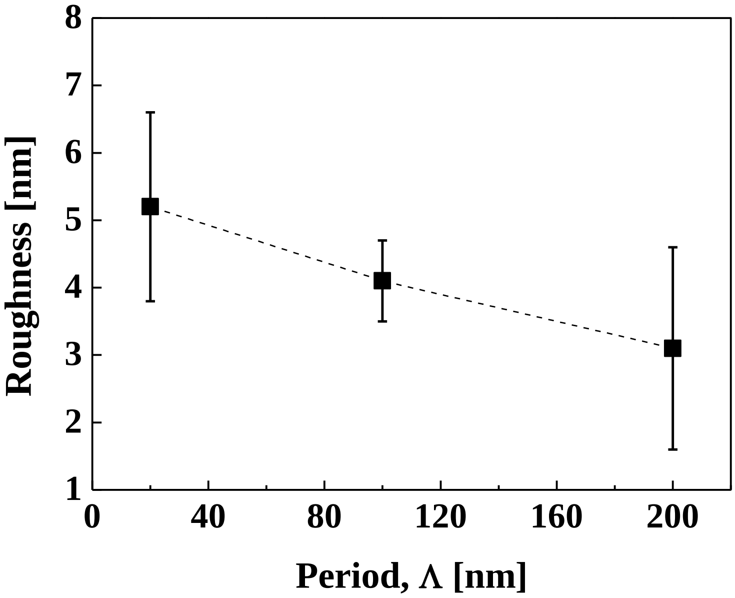

Figure 4. Roughness of CrN/Cr nano-multilayers deposited onto 304 stainless-steel substrates.

The roughness of the as-deposited films, shown in Fig. 4, exhibits a light roughness increase (~1 nm) as the bilayer period decreases, it is related to the interfacial roughness and intermixing due to layer interdiffusion during films growth, as have been reported by other studies [19,29,30]; also it is linked to the surface nodular morphology [31] as can be observed in plan-view SEM images (Fig. 2).

The atomic shadow effect generated by the geometrical restrictions is due to: growth surface roughness, growth velocity changes between columns, angle of incidence of atoms on the surface in growth and/or low adatoms mobility [6,29] and microscopic defects of the 304 ss substrate surface, these partially explain the roughness behavior in the CrN/Cr nano-multilayers of 5.2, 4.1 and 3.1 nm, for samples with bilayer period of 20 (M20), 100 (M100) and 200 nm (M200), respectively, according to AFM measurements shown in Fig. 4.

3.2 Electrochemical behavior

The corrosion behavior of 304 stainless-steel substrates uncoated and coated with 1-µm-thick CrN/Cr nano-multilayers was studied using electrochemical impedance spectroscopy (EIS). The behavior as a time function was determined following immersion for 1, 24, 48, 72 and 168 hours in 3.0% NaCl solution at room temperature. A 10 mA sinusoidal amplitude was applied to obtain current through the samples studied.

For uncoated and CrN/Cr-coated 304 ss samples after 168 h of immersion in the electrolyte, Fig. 5 shows the Bode plots. The plots relate the absolute system impedance $|Z|$ as a function of the frequency ω, shown in Fig.5a, and the phase angle shift Φ between the sinusoidal current and voltage signal as a function of the frequency ω in Fig. 5b.

For these measurements at frequencies from 10^5 to 10^0 Hz, the current was equally distributed over the whole coated area, representing the behavior of the CrN/Cr multilayers. At ω from 10^0 to 10^{-2} Hz, the current is concentrated at the substrate through the coating pores [32].

In $|Z|$ vs. ω, Fig. 5a, the uncoated 304 ss sample exhibits the lowest impedance $|Z|$, while the CrN/Cr nano-multilayer samples have up to two orders of magnitude more. In Fig. 5b, Φ vs. ω, the peak at ω from 10^4 to 10^0 Hz represents the coating capacitive behavior [33], a $\Phi = 90°$ represents the best capacitive behavior. For 304 ss substrate, the peak ($\Phi = 73.93°$; 10^1 to 10^0 Hz) is due to the formation of a thin “passive film” on its surface with ~1-3-nm-thick [9]. This passive film is composed of an outer layer OH-rich, and an inner Cr^{3+}-rich, suggesting that there are oxides (Cr_2O_3) and hydroxides [9]; thus, good corrosion performance on stainless-steels is due to the Cr enrichment of this passive film. A critical Cr content of 13% in the steel is necessary to create the stainless character [9], the 304 ss substrates employed in this research have > 18% Cr content.

For CrN/Cr films (M20; M100 and M200) in Fig. 6 (a, c and e) for $|Z|$ vs. ω, there are not significative changes as a function of the bilayer period (Λ); however, at ω from 10^{-1} to 10^{-2} Hz for M100 and M200 $|Z|$ increases as a function of time immersion, while for M20 decreases at 24 h, then increases.

For CrN/Cr films (M20; M100 and M200) in Fig. 6 (b, d and f) for Φ vs. ω, the peaks ($79.23° < \Phi < 76.96°$; 10^2 to 10^3 Hz) represents a good corrosion resistance behavior. There are not significative changes as a function of the bilayer period (Λ); however, the presence of a negative slope at high ω (10^5 to 10^3 Hz) for CrN/Cr films, indicates a better ability to retard charge transfer at the electrolyte/system interface than the 304 ss substrate at lower ω (10^3 to 10^1 Hz). This is related to the interfaces, which act like barriers blocking propagation of permeable defects, such as micro-cracks, droplets, dislocations, pinholes and pores [13], inherent to hard coatings grown by PVD techniques [6]. Dense CrO_x, Cr_2O_3

and hydroxides formation generated by Cr chemical reaction in the electrolyte, results in a passivation, with low electric conductivity and high corrosion resistance, which act like another coating, incrementing the capacitive film/substrate system. At ω from 10^1 to 10^{-2} Hz for M100 and M200 samples, there are not presence of peaks (only a positive slope) indicating that the electrolyte does not reaches the film/304 ss substrate interface, and a resistance to mass transfer between films and electrolyte through the permeable defects, called Warburg impedance, is the main driving force of the electrochemical process at low ω. This impedance is characterized by mixing processes of capacitor and resistor [34]. The M20 sample at 24 h exhibits a slight change at ω from 10^0 to 10^1 Hz related to electrolyte diffusion reaching the film/304 ss interface through permeable defects, however, after increasing due to passivation effects. The peak height at ω from 10^4 to 10^2 Hz, present in all samples studied (M20, M100 and M200), increases as a function of immersion time, indicating an improvement of the corrosion resistance due to the Cr layer oxidation and the plugging of electrolyte diffusion pathways. For M20 sample, the peak height decreases after 72 h of immersion, reducing its capacitance due to the electrolyte diffusion towards film/substrate interface, through defects at the coating. The last measurement after 168 h shows a higher resistance due to a passive layer formation in this interface. For the samples M100 and M200, at ω 10^{-2} Hz, the steady behavior of Φ can be related to lower electrolyte diffusion and a passive denser layer, incrementing the protection at this interface (film/substrate); so, a thicker bilayer period (ʌ) generates denser oxide, increasing the system corrosion resistance.

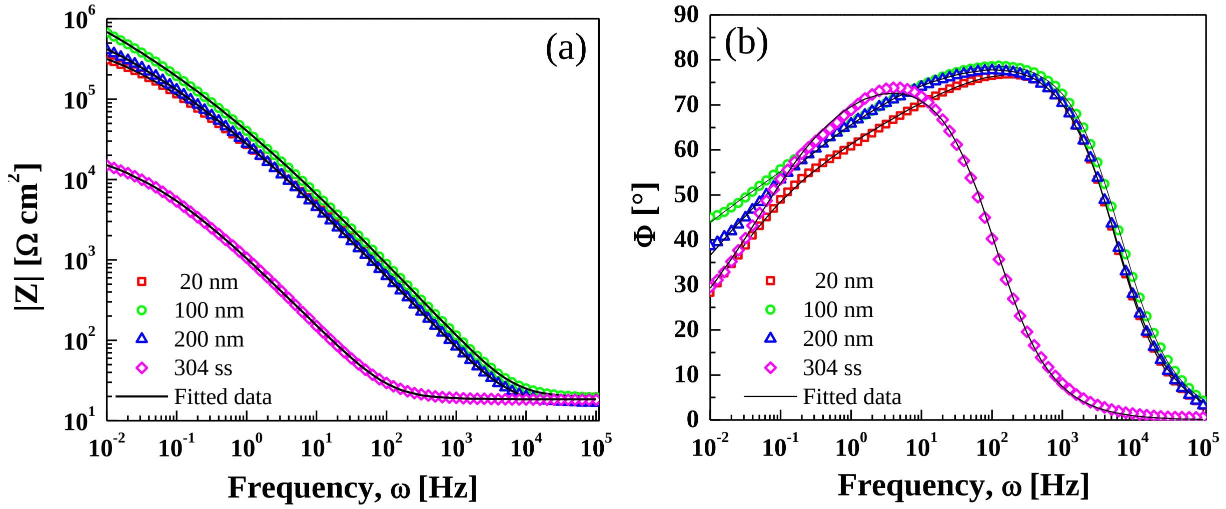

Figure 5. Experimental impedance Bode plots for (a) the absolute impedance |Z| and (b) the phase angle Φ as a function of frequency ω for the 304 stainless-steel uncoated and CrN/Cr nano-multilayers after 168 h of immersion in 3.0% NaCl solution.

To better understand the EIS results, the data were fitted with a physical model of an equivalent circuit (EC) of resistors and capacitors proposed in reference [32], for porous coatings in which corrosion processes are developed into coating permeable defects and the film/substrate interfaces. This EC shown in Fig. 7, represents the charge transport involved during the electrochemical experiment with the same amplitude and phase angle, that the real cell does under a given excitation [34]. It is composed of resistors (R) and constant phase elements (CPE), where the CPE is a mathematical expression related to electrode superficial heterogeneities and the fractal nature of the surface [23]. The CPE impedance, $Z_{CPE} = Z_0(j\omega)^{-m}$, depends on power-law m, which is 0 for pure resistance and 1 for pure capacitance. However, if m > 0.8, the CPE is treated as a capacitor [35]; thus, the CPEs made possible to obtain the best possible fits on the experimental data recorded. The reference electrode (RE) is the saturated calomel electrode (SCE), and the CrN/Cr films deposited on 304 ss substrates are the working electrode (WE).

The circuit simulates the electrochemical reactions at the electrolyte/films interface, where: R_{pore} is the pore resistance to the current flow through the film permeable defects and CPE_c is the coating constant phase element. At the electrolyte/304 ss interface, R_{ct} is the charge-transfer resistance and CPE_{ct} is the charge-transfer capacitance. The fits of the EIS data were made with Gamry Echem Analysis software [21] using the non-linear least squares method.

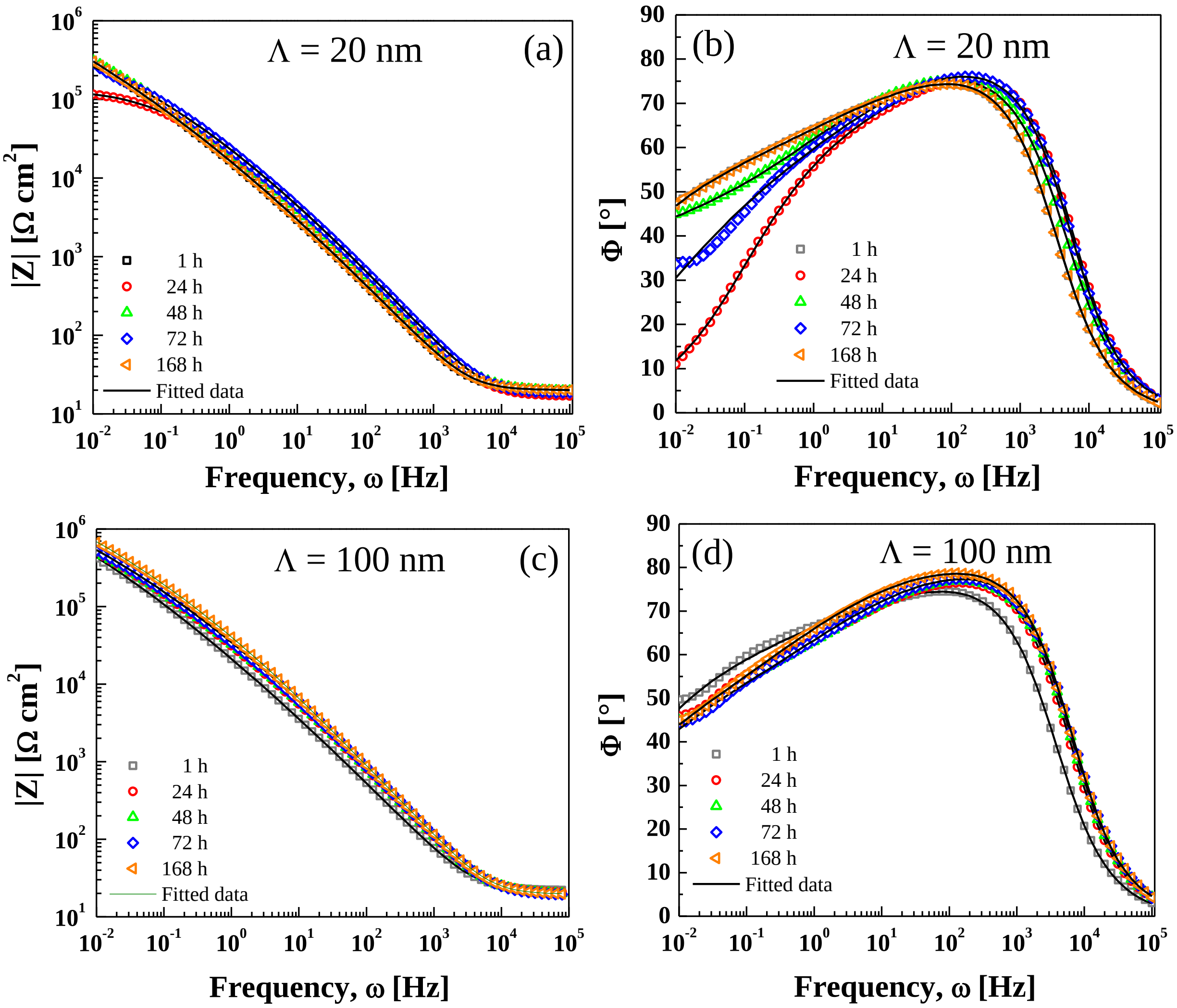

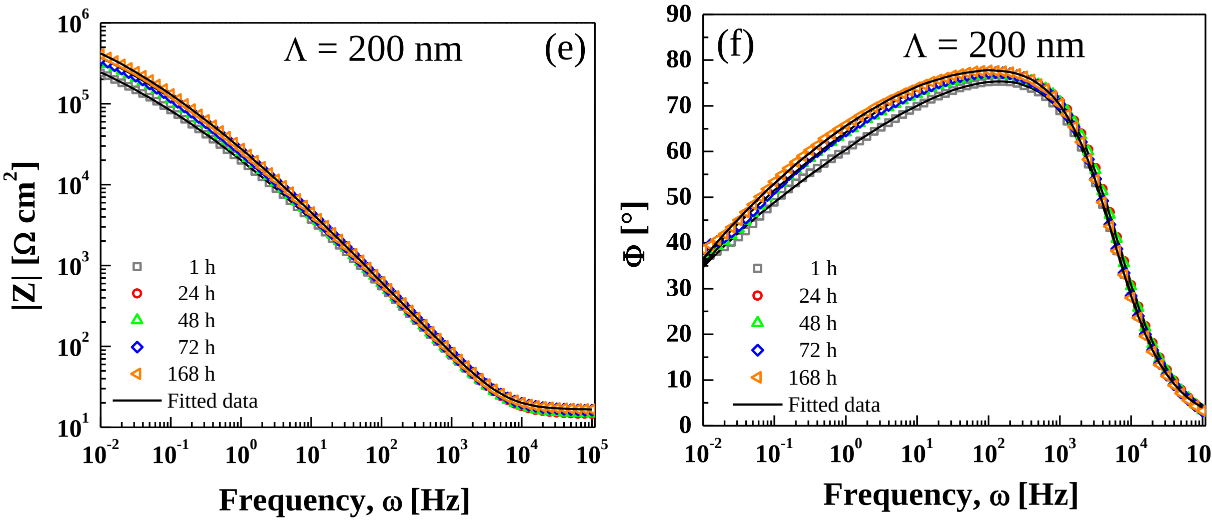

Figure 6. Experimental impedance Bode plots for (a), (c) and (e) absolute impedance |Z|, and (b), (d) and (f) angle phase Φ of EIS data obtained for CrN/Cr nano-multilayers films deposited on 304 stainless-steel substrates with period of 20 nm (a and b), 100 nm (c and d) and 200 nm (e and f).

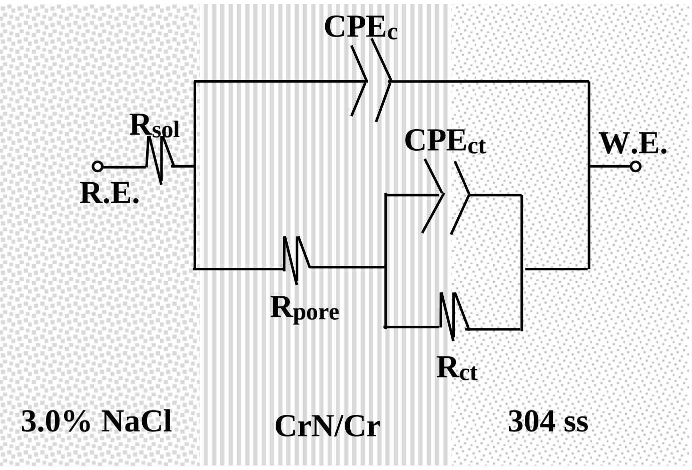

Figure 7. Equivalent circuit employed to fit EIS data for CrN/Cr nano-multilayers films and 304 ss uncoated.

Fig. 8 shows the pore resistance R_{pore} and the CPE_c through the 168 h of immersion. For all CrN/Cr samples, R_{pore} increases with time immersion. The M20 sample exhibits the larger R_{pore} increase during 168 h of measurement, which is attributed to a fast-passive film formation at the film/304 ss interface. The samples M100 and M200 show a lower R_{pore} increase related to Cr layers passivation, that as mentioned above, contributes in obtaining a larger system corrosion resistance. CPE_c has a m power-law larger than 0.9 (not shown) exhibiting a capacitive behavior two orders of magnitude lower than the 304 ss substrate uncoated (not shown), this capacitance reduction indicates that the electrolyte diffuses toward the film/304 ss substrate interface in all samples. For the sample M20, CPE_c decreases rapidly in the first 24 h of measurement due to fast electrolyte diffusion. This trend continues until 72 h because a re-passivation process, that is related to pitting of the passive film at the 304 ss surface through the coating defects. The CPE_c for the sample M100, diminishes until 48 h of measurement, while M200 do it in the first 24 h, and both show a quasi-steady behavior through to 168 h. These trends are related to the bilayer period thickness. With a thicker bilayer period the coating is more capacitive, again due to Cr layer passivation of the CrN/Cr multilayers.

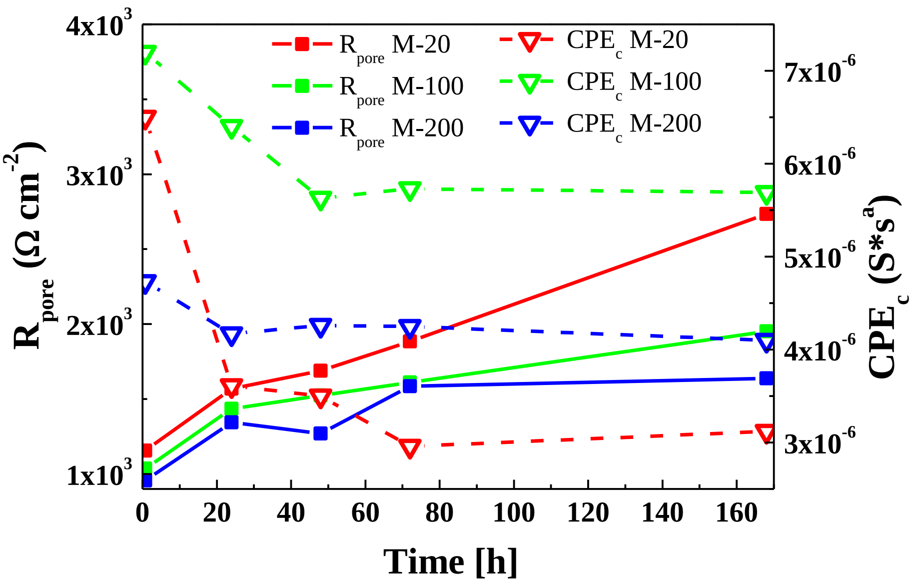

Figure 8. Pore resistance (R_{pore}) and constant phase element of the films (CPE_c), obtained from the EIS data fit for CrN/Cr nano-mutilayers and 304 stainless-steel substrates.

After 168 h of immersion, the samples were analyzed by SEM. As shown in Fig. 9, CrN/Cr nano-multilayers have porosity (pits) with no corrosion products, neither detachment or fragmentation of the films. The pores density increases with the period, indicating a greater film pitting for M200 samples due to galvanic corrosion generated by difference electrochemical potential between CrN/Cr layers and passivation products formation. By LCM, we verified the formation of pits and protuberances related to corrosion products formation and its accumulation. This confirms the pitting corrosion on these CrN/Cr nano-multilayers/304 ss systems.

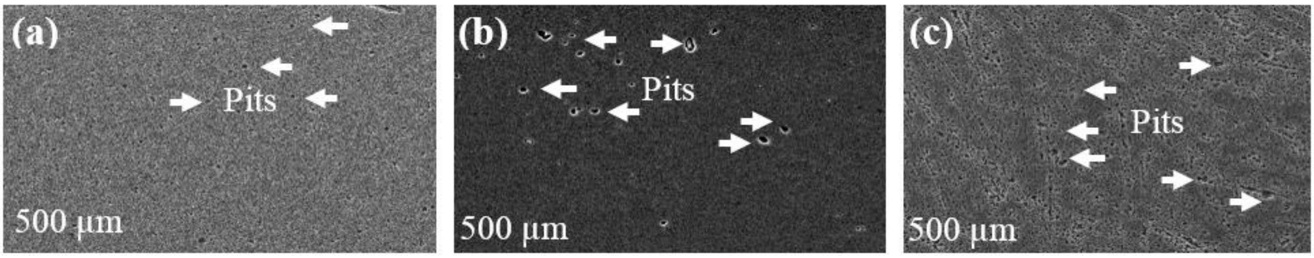

Figure 9. Plan-view SEM image of CrN/Cr nano-multilayers acquired after 168 h of immersion in the 3.0% NaCl solution at room temperature for (a) ʌ = 20 nm (M20), (b) ʌ = 100 nm (M100) and (c) ʌ = 200 nm (M200).

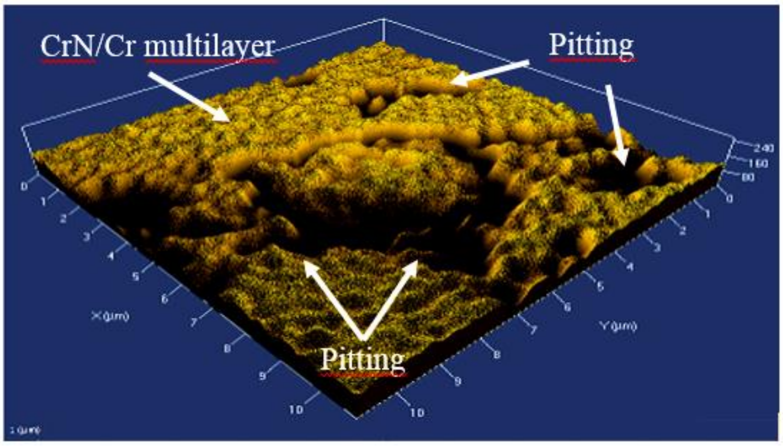

Figure 9. LCM image of CrN/Cr nano-multilayers acquired after 168 h of immersion in the 3.0% NaCl solution at room temperature.

4. CONCLUSIONS

CrN/Cr nano-multilayers films were deposited by UBMS on 304 stainless-steel substrates. Films corrosion behavior has been studied and compared with an uncoated 304 ss substrate using electrochemical impedance spectroscopy technique. The effect of the bilayer period at the CrN/Cr multilayer coating, was correlated with the corrosion resistance as indicated below.

The multilayers roughness was affected by the bilayer period, increasing with the number of interfaces and with the period reduction. It is related to layer interdiffusion during films growth.

The pore resistance R_{pore} increased for all the studied samples. Sample M20 had the larger increment, is attributed to a fast-passive film formation at the film/304 ss interface, which acts like another coating, incrementing the capacitive film/substrate system due to oxides formation (CrO_x, Cr_2O_3) effect.

At the film/substrate interface, the Warburg diffusion processes dominated due to the dense microstructure of the films and oxides formation, which protects the substrate.

ACKNOWLEDGEMENT
This research was carried out with financial support by Banco de la República de Colombia project 201010011960 and la DIB Universidad Nacional de Colombia.

References

1. S. Wang, H. Lin, H. Bor, Y. Tsai, and C. Wei, *J. Alloys Compd.*, 509 (2011) 10110.
2. H. A. Zamani and S. Sahebnasagh, *Int. J. Electrochem. Sci.*, 8 (2013) 3708.
3. Y. Hu, J. Zhu, and Y. Liu, *Int. J. Electrochem. Sci.*, 12 (2017) 11387.
4. Y. Zhao, D. Kang, Z. Chen, J. Zhan, and X. Wu, *Int. J. Electrochem. Sci.*, 13 (2018) 1250.
5. Y. L. Chipatecua, J. J. Olaya, and D. F. Arias, *Vacuum* 86 (2012) 1393.
6. D. M. Mattox, *Handbook of Physical Vapor Deposition (PVD) Processing*, p. 746, (2010).

7. W. Aperador, C. Amaya, and J. C. Caicedo, *Int. J. Electrochem. Sci.*, 8 (2013) 5275.
8. J. E. Greene, *J. Vac. Sci. Technol. A*, 35 (2017) 05C204.
9. R. K. Gupta and N. Birbilis, *Corros. Sci.*, 92 (2015) 1.
10. A. Anders, *J. Appl. Phys.*, 121 (2017) 171101.
11. A. Baptista, F. J. G. Silva, J. Porteiro, J.L. Mïguez, G. Pinto and L. Fernandes, *Procedia Manufacturing*, 17 (2018) 746.
12. A. Anders, *Surf. Coat. Techl.* 257 (2014) 308.
13. N. E. Beliardouh, K. Bouzid, C. Nouveau, B. Tlili, and M. J. Walock, *Tribol. Int.* 82 (2015) 443.
14. D. M. Marulanda, J. J. Olaya, U. Piratoba, A. Mariño, and E. Camps, *Thin Solid Films* 519 (2011) 1886.
15. A. Lousa, J. Romero, E. Martínez, J. Esteve, F. Montalà and L. Carreras, *Surf. Coat. Technol.*,146–147 (2001) 268.
16. M. Kot, W.A. Rakowski, Major, R. Major, and J. Morgiel, *Surf. Coat. Technol.*, 202 (2008) 3501.
17. L. Cunha, M. Andritschky, L. Redouta and K. Pischow, *Surf. Coat. Technol.*, 116 (1999) 1152.
18. S. Kaciulis, A. Mezzi, G. Montesperelli, F. Lamastra, M. Rapone, F. Casadei, T. Valente and G. Gusmano, *Surf. Coat. Technol.*, 201 (2006) 313.
19. J. Romero, J. Esteve, and A. Lousa, *Surf. Coat. Technol.*, 188–189 (2004) 338.
20. E. Martinez, J. Romero, a. Lousa, and J. Esteve, *Surf. Coat. Technol.*, 163–164 (2003) 571.
21. Echem Analyst Software, (2011).
22. D. Bhattacharyya, N. A. Mara, P. Dickerson, R. G. Hoagland, and A. Misra, *Acta Mater.*, 59 (2011) 3804.
23. E. Vogli, W. Tillmann, U. Selvadurai-lassl, G. Fischer, and J. Herper, *Appl. Surf. Sci.* 257 (2011) 8550.
24. B. Subramanian, R. Ananthakumar, V. S. Vidhya, and M. Jayachandran, *Mater. Sci. Eng. B* 176 (2011) 1.
25. P. Panjan, M. Čekada, M. Panjan, and D. Kek-Merl, *Vacuum* 84 (2009) 209.
26. Y. X. Ou, J. Lin, S. Tong, W. D. Sproul, and M. K. Lei, *Surf. Coat. Technol.*, 293 (2016) 21.
27. P. Wiecinski, J. Smolik, H. Garbacz, and K. J. Kurzyd, *Surf. Coat. Technol.*, 240 (2014) 23.
28. J. A. Thornton, *Annu. Rev. Mater. Sci. 7*259 (1977).
29. R. F. Bunshah, L. Hultman and J.E. Sundgren, *Handbook of hard coatings. Structure/property relationships for hard coatings*, chapter 4 (2001), United States of America: Noyes Publications.
30. A. Biswas and D. Bhattacharyya, *J. Appl. Phys.*, 109 (2011) 084311.
31. J. Creus, E.H. Top, C. Savall, Ph. Refait, C. Ducros and F. Sanchette, *Surf. Coat. Technol.*, 202 (2008) 4047.
32. C. Liu, Q. Bi, A. Leyland, and A. Matthews, *Corros. Sci.* 45 (2003) 1243.
33. C. Liu, Q. Bi, A. Leyland, and A. Matthews, *Corros. Sci.* 45 (2003) 1257.
34. A. J. Bard, *Elctrochemical methos, Fundamentals and Applications*, p. 3-7, (1944), United States of America: John Wiley & Sons, INC.
35. C. Liu, Q. Bi, and A. Matthews, *Corros. Sci.,* 43 (2001) 1953.